

Performance of a hybrid PV/T double-pass finned plate solar air heater

A. A. El-Sebaei¹, A. M. Khallaf², M. R. I. Ramadan¹, S. Aboul-Enein¹, M. M. Hegazy^{1, *}

¹Department of Physics, Faculty of Science, Tanta University, Tanta, Egypt

²Department of Basic Science, Misr Higher Institute for Engineering and Technology, Mansoura, Egypt

*Corresponding Author: Tel.: +20 1226803483,

E-mail address: mohammedmossad7070@gmail.com (M. M. Hegazy)

The hybrid (PV/T) double flow pass air heater with finned absorber was investigated theoretically. In this model, the air flows through the heater from the upper flow duct and comes out from the lower flow duct after circulation. The considered PV unit is utilized to deliver the electrical power necessary to actuate the pump and blow the air through the upper and lower ducts. The impact of \dot{m} on the outlet temperature, thermal and electrical output powers and overall efficiency have been studied. The DPFPSAH has been investigated with and without the PV module. Additionally, the impact of using fins on the heater performance has been discussed. The experimental outcomes display that the electrical power of the PV unit can run the fan and blow the air at \dot{m} lower than 0.37 kg/s. The thermal efficiency has been increased from 30% at \dot{m} 0.006 kg/s to 70% at \dot{m} 0.06 kg/s, while the electrical efficiency has been increased from 6.4% to 7.3% at the same mass flow rates.

1. Introduction:

A PV/T heater contains a PV unit to generate electricity and a solar heater to produce heat [1,2]. There are two types of (PV/T) solar collectors relying upon the operative fluid; PV/T solar air heaters and PV/T solar water heaters. The PV/T air heaters have benefits over the PV/T water heaters, including (i) no corrosion (ii) less leakage through joints and ducts (iii) compact system, and simple in setup. Nevertheless, there are few drawbacks of using air as a working fluid such as the low thermal conductivity of air, so stretched surfaces such as fins are utilized to

expand the area and augment the overall rate of heat transfer [3]. Hussain et al. [1] made an enhancement of a PV/T design by adding a hexagonal honeycomb heat exchanger. The system was tried with and without the honeycomb at solar irradiance of 828 W/m^2 and \dot{m} going from 0.02 to 0.13 kg/s. They found that, at a \dot{m} of 0.11 kg/s, the thermal efficiency is 27 % without the honeycomb and 87 % with the honeycomb. Ahmed et al. [4] showed that the dust affects the performance of the hybrid PV/T solar collector. They indicated that the dust decreases the thermal efficiency by 13.4 % and the topmost electrical efficiency was 10.24% when the collector is clean and 5.67 % when the dust is present. Moreover, the dust decreased the total efficiency by 17.5 %. Hegazy [5] made a comparison between four distinctive designs of hybrid PV/T air heaters. In the first design, the air streamed over the absorbent surface. The second design is opposite to the first design as the air streamed down the absorbent surface. In the third one, the air pumped above and below the absorbent surface in a single track, while in the fourth design, the air recycled through the ducts. He concluded that the first design has the minimal performance in comparison with the other designs which have nearly the same performance. Moreover, the third design demanded the least power compared to the second and fourth designs. Coventry [6] examined the concentrating hybrid PV/T air heater. He concluded that the thermal efficiency of the examined PV/T system was 58 % while the electrical efficiency was 11 %. This provided an overall efficiency about 69%. The PV/T solar system with and without a cover of glass was studied by Shams and Ameri [7]. The outcomes displayed that the thermal efficiency increases in the presence of the glass cover while the electrical efficiency of the system decreases. Ahmed et al. [8] examined the impact of utilizing a porous medium on the performance of a hybrid PV/T system. The outcomes showed that the most elevated estimation of the daily thermal efficiency was 80.3% in the presence of the porous medium.

To get superior electrical efficiency, Dubey et al. [9] contemplated four distinct designs of PV modules specifically; (a) Glass-glass PV module with duct, (b): Glass-glass PV module without duct, (c): Glass-Tedlar PV module with duct, (d): Glass-Tedlar PV module without duct. They inferred that design (a) provides the topmost electrical efficiency and outlet temperature. The yearly average electrical efficiency in case of glass-glass type with and without duct was 10.41 % and 9.75 %, respectively. Othman et al. [10] studied a hybrid PV/T system consists of a group of solar cells, concentrator and a finned absorber. By comparing the theoretical results with the experimental, they found a great agreement and concluded that the produced electricity decreases with raising the temperature of the flowing air. Tiwari and Sodha [11] studied the single pass PV/T air heater with air passing under the absorbent surface, a glass cover and a tedlar on the back of the solar cells. It was seen that the single pass glassed heater without tedlar gave the topmost performance.

In this study, the PV/T (DPFPSAH) has been contemplated. Galvanized iron rectangular fins are appended on the back face of the absorbent surface.

The purpose of this study is:

- 1- The comparison the performance of the PV/T (DPFPSAH) with and without the PV unit.
- 2- Calculation of the daily electrical output power necessary to run the fan and blow the air through the heater.

Impact of \dot{m} of air on assorted parameters like thermal, electrical and overall efficiencies and useful thermal and electrical output powers has been negotiated.

2.Theoretical analysis

The hybrid PV/T DPFPSAH is displayed in figure (1). It contains a glass cover, an absorbent surface made of a 1m^2 galvanized iron sheet with a PV module mounted on the upper face of it. Rectangular fins are appended on the back face of the absorbent surface to boost the transfer rate of heat. For easiness, the energy balance equations of different parts of the heater are articulated below the next suggestions: (a) There is a perfect connection between the PV unit and the absorbent surface, thus they have equal temperatures. (b) The glass sheet, the absorbent surface and the back plate have marginal heat capacities. (c) there is no air infiltration as the system is assumed to be compact. (d) The heater is assumed to be operated in a steady state. (e) The running air temperature changes only in the side of flow.

For the back plate:

$$A_b h_b (T_{fl} - T_b) + A_b h_{rpb} (T_p - T_b) = A_b U_b (T_b - T_a) \tag{6}$$

where ($U_b = k_b/x_b$) is back heat loss coefficient due to conduction ($W/m^2 k$).

For the running air in the upper duct, the energy balance equation for a unit length dx can be indicated as:

$$bdx h_{p1} (T_p - T_{fu}) = \dot{m}_{fu} C_{fu} \frac{dT_{fu}}{dx} dx + bdx h_{cg} (T_{fu} - T_g) + bdx U_s (T_{fu} - T_a) \tag{7}$$

where ($U_s = k_s/x_s$) is the side heat loss coefficient due to conduction ($W/m^2 k$).

For the running air in the lower duct:

$$bdx h_{p2} \phi (T_p - T_{fl}) = \dot{m}_{fl} C_{fl} \frac{dT_{fl}}{dx} dx + bdx h_b (T_{fl} - T_b) + bdx U_s (T_{fl} - T_a) \tag{8}$$

Where ϕ and η_{fin} are expressed using the next formulas [13]:

$$\phi = 1 + \left(\frac{A_{fin}}{A_p}\right) \eta_{fin} , \tag{9}$$

and

$$\eta_{fin} = \frac{\tanh \sqrt{2hH/k_{fint}}}{2hH/k_{fint}} . \tag{10}$$

The sky temperature T_s is calculated using Swinbank formula [14] as:

$$T_s = 0.0552 T_a^{1.5} . \tag{11}$$

The wind heat transfer coefficient h_w is computed from [14]:

$$h_w = 5.7 + 3.8V \tag{12}$$

where V is the velocity of wind (m/s).

The heat transfer coefficient due to radiation from the glass to the sky is calculated from [15]:

$$h_{rgs} = \epsilon_g \sigma (T_g^2 + T_s^2)(T_g + T_s) . \tag{13}$$

The heat transfer coefficient due to radiation from the absorbent surface to the glass cover is calculated from the equation[14]:

$$h_{rpg} = \frac{\sigma(T_p^2 + T_g^2)(T_p + T_g)}{\left(\frac{1}{\epsilon_p}\right) + \left(\frac{1}{\epsilon_g}\right) - 1} \tag{14}$$

The heat transfer coefficient due to radiation from the absorbent surface to the back plate can be computed from the equation[14]:

$$h_{rpb} = \frac{\sigma(T_p^2 + T_b^2)(T_p + T_b)}{\left(\frac{1}{\epsilon_p}\right) + \left(\frac{1}{\epsilon_b}\right) - 1} \tag{15}$$

The heat transfer coefficient h_{p1} from the absorbent surface to the air streaming through the upper channel is suggested to be equal to the heat transfer coefficient from the streaming air in the upper channel to the glass cover h_{cg} [16].

$$h_{p1} = h_{cg} = \frac{Nu_{fr} k_{fu}}{D_{hu}}, \quad (16)$$

where k_{fu} is the thermal conductivity (W/m K) of the air running in the upper flow duct, Nu_{fr} is the Nusselt number for forced convective operation mode and D_{hu} is the hydraulic diameter (m) of the upper flow duct which can be computed from [14]:

$$D_{hu} = 2bd_{fu} / (b + d_{fu}), \quad (17)$$

where d_{fu} is the depth of the upper flow channel.

The Nusselt number for forced convective operation mode Nu_{fr} is given as:

For laminar flow ($Re < 2300$) [17]:

$$Nu_{fr} = 5.4 + \frac{a[Re Pr (\frac{D_h}{L})]^m}{1+c[Re Pr (\frac{D_h}{L})]^n}, \quad (18)$$

where

$Pr = 0.7$ is Prandtl number. While a , c , m and n are constant quantities equal 0.0019, 0.00563, 1.71 and 1.17, respectively.

For turbulent flow ($Re > 2300$) [18]:

$$Nu_{fr} = 0.0158 Re^{0.8} \quad (19)$$

where Re is the Reynold's number computed by the next formula [21]:

$$Re = \frac{2\dot{m}}{\mu (b+d_f)} \quad (20)$$

The dynamic viscosity of the running air μ in (kg/m s) and d_f is flow channel depth.

It was suggested that the heat transfer coefficient h_{p2} is equal to the convective heat transfer coefficient from the streaming air in the lower channel to the back plate h_b [18] and they are computed by the equation given for h_{p1} (Eq.16).

Upon some mathematical procedures, the next formulas for T_g, T_p and T_b are given as:

$$T_g = n_1 + n_2 T_{fu} + n_3 T_{fl} + n_4 T_a + n_5 T_s . \tag{21}$$

$$T_p = n_6 + n_7 T_{fu} + n_8 T_{fl} + n_9 T_a + n_{10} T_s . \tag{22}$$

$$T_b = n_{11} + n_{12} T_{fu} + n_{13} T_{fl} + n_{14} T_a + n_{15} T_s . \tag{23}$$

The values of n's coefficients in Eqs. (21, 22 and 23) are given in Appendix A
 Substituting T_g, T_p and T_b using Eqs. (21), (22) and (23), Eqs. (7) and (8) become

$$\frac{dT_{fu}}{dx} = -A_1 T_{fu} + E_1 T_{fl} + f_1(t). \tag{24}$$

$$\frac{dT_{fl}}{dx} = -A_2 T_{fl} + E_2 T_{fu} + f_2(t). \tag{25}$$

Where the coefficients $A_1, A_2, E_1, E_2, f_1(t)$ and $f_2(t)$ are given in Appendix B.

With the elimination method [20], Eqs. (24) and (25) are solved. Assuming $f_1(t)$ and $f_2(t)$ have average values $\overline{f_1(t)}$ and $\overline{f_2(t)}$ throughout a period span from 0 to t and possibly considered as constants [21].

From Eq. (25) we have

$$T_{fu} = \frac{1}{E_2} \left[\frac{dT_{fl}}{dx} + A_2 T_{fl} - \overline{f_2(t)} \right]. \tag{26}$$

Substituting from Eq. (26) into Eq. (24), we can get

$$\frac{d^2 T_{fl}}{dx^2} + (A_1 + A_2) \frac{dT_{fl}}{dx} + (A_1 A_2 - E_1 E_2) T_{fl} = A_1 \overline{f_2(t)} + E_2 \overline{f_1(t)}. \tag{27}$$

The solution of Eq.(27) might be written as [22]

$$T_{fl} = T_{par} + T_{comp} \tag{28}$$

where T_{par} and T_{comp} are the particular and the complimentary solutions, respectively.

Assuming Ω is the differential operator, then the solution of Eq. (27) is:

$$\Omega^2 + (A_1 + A_2)\Omega + (A_1 A_2 - E_1 E_2) = 0 \tag{29}$$

The solution of Eq. (29) is given by

$$\Omega_{1,2} = \frac{-(A_1 + A_2) \pm \sqrt{(A_1 + A_2)^2 - 4(A_1 A_2 - E_1 E_2)}}{2}. \tag{30}$$

And the complementary solution T_{comp} is given by

$$T_{comp} = C_1 e^{\Omega_1 X} + C_2 e^{\Omega_2 X}, \tag{31}$$

where C_1 and C_2 are constants.

The temperature of the air coming out from the upper duct T_{fu0} equals the temperature of the air that enters the lower duct T_{fli} during circulation at $x = L$. So the constants C_1 and C_2 are given by:

$$C_1 = \frac{E_2 T_{fui} - (\Omega_2 + A_2) T_{fu0} + \Omega_2 T_{par} + \overline{f_2(t)}}{\Omega_1 - \Omega_2}. \tag{32}$$

$$C_2 = \frac{(\Omega_1 + A_2) T_{fu0} - E_2 T_{fui} - \Omega_1 T_{par} - \overline{f_2(t)}}{\Omega_1 - \Omega_2}. \tag{33}$$

T_{par} is suggested to be a constant because, the non-homogeneous part of Eq.(27) is a constant [22].so the particular solution is obtained as

$$T_{par} = \frac{A_1 \overline{f_2(t)} + E_2 \overline{f_1(t)}}{A_1 A_2 - E_1 E_2}. \tag{34}$$

By substitution from Eq. (34) into Eq. (26), we get

$$T_{fu}(x) = \frac{1}{E_2} [(\Omega_1 + A_2) C_1 e^{\Omega_1 x} + (\Omega_2 + A_2) C_2 e^{\Omega_2 x} + A_2 T_{par} - \overline{f_2(t)}] \tag{35}$$

The outlet T_{fuo} and average T_{fuav} temperatures of the streaming air in the upper duct are obtained as

$$T_{fuo} = T_{fu}(x) \Big|_{x=L} = \frac{1}{E_2} [(\Omega_1 + A_2)C_1 e^{\Omega_1 L} + (\Omega_2 + A_2)C_2 e^{\Omega_2 L} + A_2 T_{par} - \overline{f_2(t)}] . \quad (36)$$

and

$$T_{fuav} = \frac{1}{L} \int_0^L T_{fu}(x) dx = \left(\frac{1}{LE_2} \right) [(\Omega_1 + A_2) \frac{C_1}{\Omega_1} (e^{\Omega_1 L} - 1) + (\Omega_2 + A_2) \frac{C_2}{\Omega_2} (e^{\Omega_2 L} - 1) + A_2 L T_{par} - L \overline{f_2(t)}] . \quad (37)$$

Also, the outlet T_{flo} and average T_{flav} temperatures of the streaming air in the lower duct are calculated as

$$T_{flo} = T_{fl}(x) \Big|_{x=2L} = C_1 e^{2L\Omega_1} + C_2 e^{2L\Omega_2} + T_{par} \quad (38)$$

and

$$T_{flav} = \frac{1}{2L} \int_0^{2L} T_{fl}(x) dx = \left(\frac{1}{2L} \right) \left[\frac{C_1}{\Omega_1} (e^{2L\Omega_1} - 1) + \frac{C_2}{\Omega_2} (e^{2L\Omega_2} - 1) + 2L T_{par} \right] . \quad (39)$$

2.1. Parameters influencing the performance of the hybrid PV/T (DPFPsAH):

A software program was created to tackle the energy balance to examine the elements influencing the performance of the proposed model, which incorporate temperature distribution, thermal, electrical, and electro-hydraulic efficiencies and furthermore electrical, thermal, and pumping powers.

The overall thermal output power is computed by [23]

$$\dot{Q}_u = \dot{m}_f C_f (T_{flo} - T_{fui}) . \quad (40)$$

The electrical output power is computed by [5]:

$$\dot{Q}_p = \eta_c \alpha_c \tau_g^2 F A_p I . \quad (41)$$

The instantaneous thermal efficiency η_T is computed by [24]:

$$\eta_T = \frac{\dot{Q}_u}{I A_p} = F_r \left[(\tau_g \alpha_p) - \frac{U_l (T_{flo} - T_{fui})}{I} \right] . \quad (42)$$

Where F_r and U_l are the efficiency factor and overall heat loss coefficient (W/m² K) of the heater, respectively.

The daily thermal efficiency η_{T-d} of the system is given as

$$\eta_{T-d} = \frac{\dot{m}_f C_f \Sigma (T_{flo} - T_{fui})}{A_p \Sigma I} . \quad (43)$$

The electrical efficiency is given as [24]:

$$\eta_E = \frac{\dot{Q}_p}{A_c I} \quad (44)$$

We can't compute the overall efficiency by summing both electrical and thermal efficiencies; and accordingly, the conversion factor of the efficiency C_f suggested by Joshi et al. [25] being able to compute the overall efficiency with big precision

and its value in most systems is taken to be in the range of 0.35 and 0.40. Through current study, C_f is proposed to be 0.40.

Accordingly, the overall efficiency is computed by [25]:

$$\eta_{overall} = \frac{\eta_E}{C_f} + \eta_T . \tag{45}$$

The fan demands an electrical power to pump the air into the heater, therefore we can suggest that the efficiencies of the motor and the fan are 90 % and 70 %, respectively [23]. Thus, the power of the fan P_{fan} and the flow pumping power P_{flow} can be estimated as [23]:

$$P_{fan} = P_{flow}/(\eta_{fan}\eta_{motor}), \tag{46}$$

$$P_{flow} = \dot{m}\Delta P/\rho, \tag{47}$$

Where the density of the streaming air ρ in (kg/m³).

ΔP is the overall pressure drop in (N/m²) and could be computed by adding the pressure drop through flow channels ΔP_{ch} and the loss through duct joints ΔP_{joints} [26].

$$\Delta P = \Delta P_{ch} + \Delta P_{joints} , \tag{48}$$

where

$$\Delta P_{ch} = 2\rho fV^2L/D_h , \tag{49}$$

$$\Delta P_{joints} = K\rho V^2/2 , \tag{50}$$

and

$$V = \dot{m}/(\rho b d_f). \tag{51}$$

K equals 2.2 like a former work [27].

For a smooth channel f is computed by [28]:

$$f = 16/Re , \quad \text{for laminar flow} \tag{52}$$

$$= 0.059Re^{-0.2} \quad \text{for turbulent flow} \tag{53}$$

For a finned channel f is computed by [29]:

$$f = 24/Re , \quad \text{for laminar flow} \tag{54}$$

$$= 0.079Re^{-0.25} \quad \text{for turbulent flow} \tag{55}$$

In the event that we suppose nearly 30 % of the electrical power is dissipated in the charge controller, cables, and inverter then about 70 % of this power is saved so the useful electrical power is just 56 % [5].

$$\text{Hence } \dot{Q}_{useful} = 0.56\dot{Q}_p . \tag{56}$$

The net available electrical power is given by:

$$\dot{Q}_{NET} = 0.56\dot{Q}_p - P_{fan} . \tag{57}$$

The electro-hydraulic efficiency can be computed as [5]

$$\eta_{e-h} = \dot{Q}_{NET}/(F I A_p) . \tag{58}$$

The top heat loss coefficient is given by [30]:

$$U_t = \left\{ \frac{N}{\left(\frac{C}{T_p}\right)\left[\frac{T_p-T_a}{(N+S)^e}\right]} + \frac{1}{h_w} \right\}^{-1} + \frac{\sigma(T_p+T_a)(T_p^2+T_a^2)}{\frac{1}{\varepsilon_p+0.00591Nh_w} + \frac{2N+S-1+0.133\varepsilon_p-N}{\varepsilon_g}} \tag{59}$$

where N is number of transparent covers, C = 520(1 - 0.000051β²);

β is the heater tilt angle, $f = (1 + 0.089h_w - 0.1166h_w \varepsilon_p)(1 + 0.07866 N)$;
 $e = 0.430[1 - (100/T_p)]$.

3.Procedure of mathematical computations

Energy balance equations for various components of the studied system are tackled with an appropriate Pascal program. The weather conditions are considered for Tanta on a mid-year day (13/6/2015). The temperatures of the PV module, glass, absorbent surface, and the streaming air are firstly speculated. The input air temperature is thought to be equivalent to the surrounding temperature. utilizing these primary temperatures, all inner and outer heat transfer coefficients were determined for figuring the temperatures of different components of the heater. The former steps were rerun using the updated estimations of the distinctive heat transfer coefficients till the total temperatures were determined along the 24 hours. The electrical and thermal powers, in addition of electrical, thermal and overall efficiencies, were then computed. The assorted thermo-physical parameters utilized in the computations have been summed up in Table 1.

Table (1) thermo-physical parameters utilized for mathematical computations

parameter	Value	parameter	Value
α_p	0.95	τ_g	0.90
α_g	0.05	$K_s = K_b$	0.059 (W/m K)
ε_p	0.90	k_f	0.026 (W/ m K)
ε_g	0.88	c_f	1006 (J/kg K)
ε_b	0.90	ρ_f	1.204(kg/m ³)

4. Results and discussions

4.1. The temperature distribution of various elements of the system

Figures 2 A and B show the hourly fluctuations of the calculated temperatures of various components of the hybrid PV/T air heater using the values of solar irradiance and ambient temperature recorded at 13/6/2015 when $\dot{m}_{fu} = \dot{m}_{fl} = 0.02 \text{ kg/s}$, $L = b = 1 \text{ m}$, $A_m = 0.5 \text{ m}^2$, $d_{fu} = d_{fl} = 0.08 \text{ m}$ and $x_b = x_s = 0.05 \text{ m}$. From Fig. 2.A, it is obvious that the solar irradiance increases with time and reaches its maximum value of 932 W/m^2 at 1.0 pm. Also, it is seen that the greatest values of T_{fuav} , T_{flav} and T_{f10} are found to be 35.5 , 49.8 , and 58.8°C , respectively.

The average temperature of the air streaming in the lower duct T_{flav} is bigger than that of air streaming in the upper duct because of circulation and fins. Fig. 2.B shows that the maximum values of T_g, T_b are 44.6 °C and 72.8 °C, respectively. The topmost temperature of the absorber surface equals 85.4 °C.

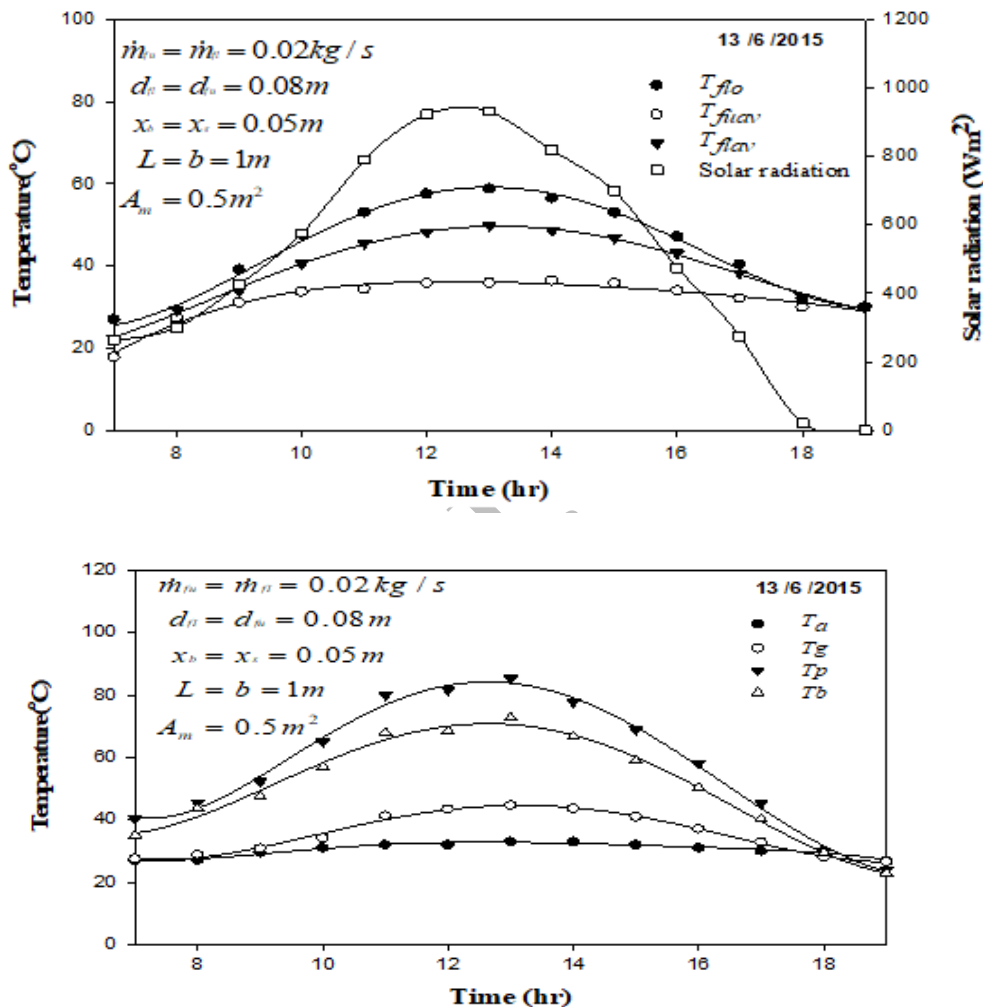


Fig.2 (A&B) Temperature distribution of various components of the hybrid PV/T (DPFPSAH).

4.2. Effect of the PV module on the DPFPSAH performance

Figure 3 presents the maximum outlet temperature $T_{flo,max}$ of the collector with and without the PV module versus \dot{m} . It is evident that in both cases, $T_{flo,max}$ declining with raising \dot{m} because of the increased heat capacity of air with \dot{m} .

Figure 3 also shows that $T_{f_{lo,max}}$ in case of the collector without the PV module is higher than when using the PV module due to the reduction in the collector area with the PV module. The outcomes indicate that the PV module reduces $T_{f_{lo}}$ by an average value of 7.8 %.

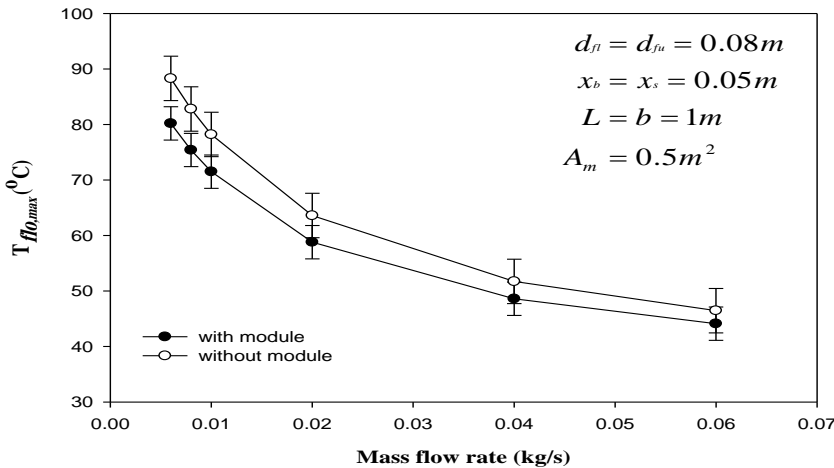


Fig.3 Maximum outlet temperature $T_{f_{lo,max}}$ of the collector with and without the PV module versus \dot{m} .

Figure 4 introduces a comparison between the daily thermal output power $\dot{Q}_{u,daily}$ of the DPFPSAH with and without the PV module. It is clear that $\dot{Q}_{u,daily}$ of the heater without the PV module is higher compared to the collector with the PV module because of the higher outlet temperature $T_{f_{lo}}$ of the collector without the PV module compared to that of the collector with the PV module. $\dot{Q}_{u,daily}$ grows up with raising \dot{m} to 0.26 kg/s then the expand turns irrelevant for both systems. For the DPFPSAH without the PV module, $\dot{Q}_{u,daily}$ is found to be increased from 3629 to 6735 Wh/day with increasing \dot{m} from 0.01 to 0.26 kg/s. Whereas it is increased from 6735 to 6773 Wh/day with increasing \dot{m} from 0.26 to 0.34 kg/s. For the DPFPSAH with the PV module, it is found that, $\dot{Q}_{u,daily}$ increases from 2064 to 5425 Wh/day with \dot{m} ranges from 0.01 to 0.26 kg/s, and is increased from 5425 to 5471 Wh/day when \dot{m} is increased from 0.26 to 0.34 kg/s. On the other hand, Fig. 4 also presents the variation of the daily electrical output power $\dot{Q}_{p,daily}$ with \dot{m} . It is found that $\dot{Q}_{p,daily}$ increases with increasing \dot{m} until 0.18 kg/s then the increase becomes trivial. $\dot{Q}_{p,daily}$ is found to increase from 221 to 276 Wh/day when \dot{m} is raised from 0.01 to 0.18 kg/s

but with \dot{m} extent from 0.18 to 0.34 kg/s, $\dot{Q}_{p,daily}$ is only increased from 276 to 282 Wh/day.

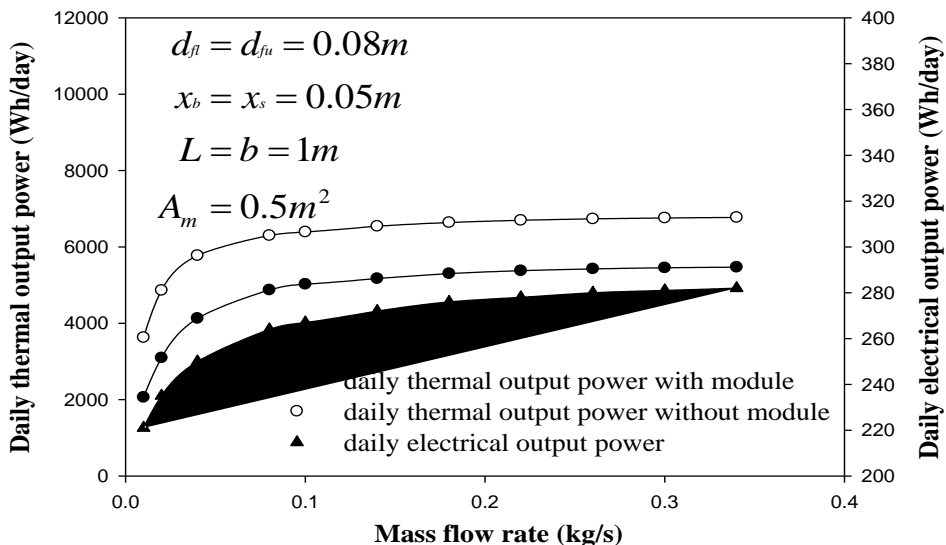


Fig.4 Daily thermal and electrical output powers.

Figure 5 shows η_T of the collector at several values of \dot{m} . Clearly, η_T increases with raising \dot{m} because of the decreased collector temperature with increasing \dot{m} . Fig.5 also indicates that η_T in case of the collector without the PV module is higher compared to the collector with the PV module owing to the higher \dot{Q}_u of the collector without the PV module. The PV module decreases η_T by an average value about 17%. The decrease in η_T will be compensated in generating the power in order to actuate the pump and blow the air through the heater.

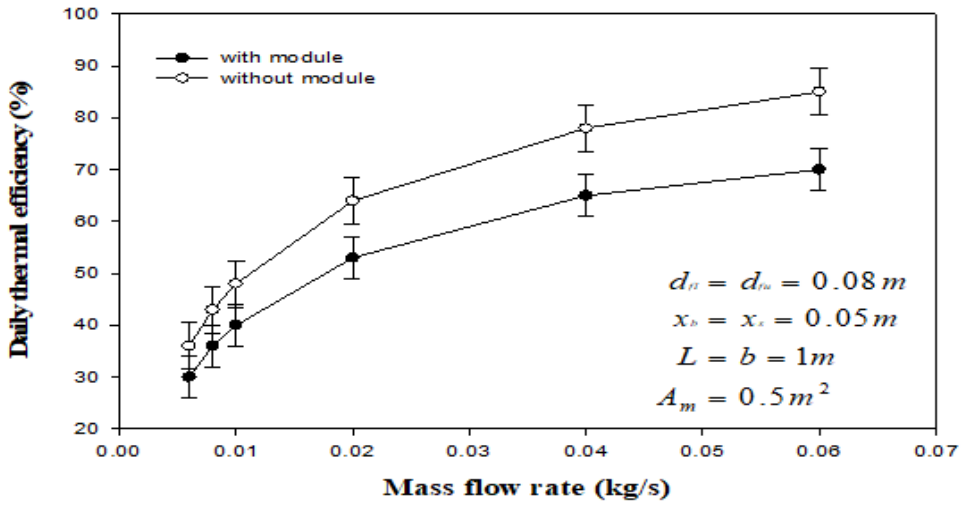


Fig.5 Thermal efficiency of the collector with several values of \dot{m} .

Figure 6 presents the change of electrical, thermal and overall efficiencies of the studied system at several values of \dot{m} . It is shown that with increasing \dot{m} , all efficiencies are increased. It is also clear that η_T is increased from 30 % at $\dot{m} = 0.006\text{ kg/s}$ to 70 % at $\dot{m} = 0.06\text{ kg/s}$, while η_E is increased from 6.4 % at $\dot{m} = 0.006\text{ kg/s}$ to 7.3 % at $\dot{m} = 0.06\text{ kg/s}$. Then $\eta_{overall}$ is increased from 46 % to 88 % at the same \dot{m} .

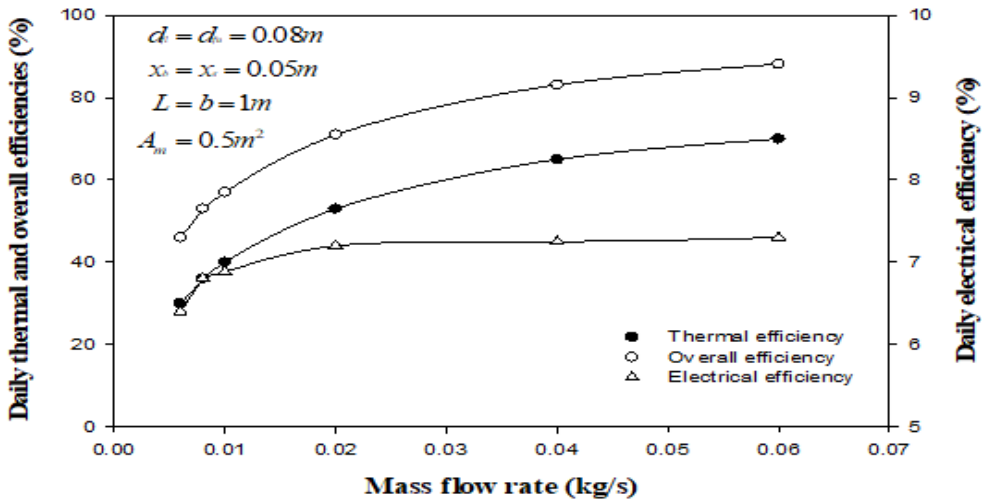


Fig.6 Change of electrical, thermal and overall efficiencies with \dot{m} .

4.3. Fins effectiveness on the performance of the studied system.

To boost the electrical efficiency, the temperature of the PV unit must be low, thus, fins are utilized to reduce the absorbent surface temperature through the improvement in its heat capacity and accordingly the PV module temperature diminishes, then η_E is increased. Also, fins are utilized to improve the heat transfer rate and increase the outlet temperature T_{f1o} .

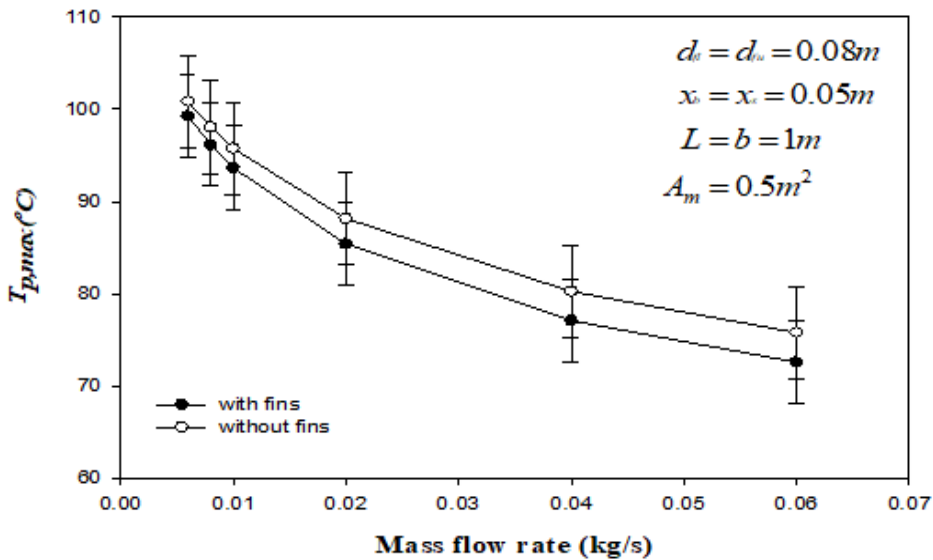


Fig.7 T_p at several values of \dot{m} with and without fins.

Variations of the absorber plate temperature T_p at several values of \dot{m} with and without fins are presented in Fig.7. It is evident that the fins reduce T_p because of the increment in its heat capacity. By keeping the PV module at low temperature, η_E is increased as in Fig.8 where η_E is increased by 10% due to the existence of the fins. Moreover, the results show that the fins increase η_T by about 8%. The same outcomes are obtained by Kumar and Rosen [31].

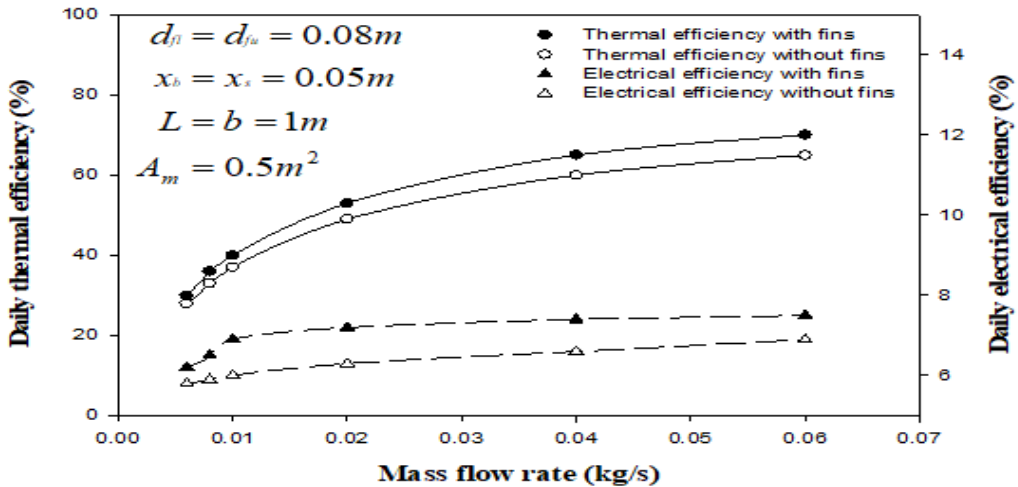


Fig.8 Comparison between thermal and electrical efficiencies with and without fins.

4.4. Effect of \dot{m} on fan and module powers

Figure 9 shows the changes of the daily fan ($P_{fan,daily}$) and module ($\dot{Q}_{p,daily}$) powers with different values of \dot{m} . It is clear that this system could provide the electrical power wanted to run the fan and blow air through the heater till \dot{m} reaches 0.37 kg/s beyond which the fan power surpasses the module power. Accordingly, it is appropriate to utilize this system with \dot{m} equals or lower than 0.37 kg/s.

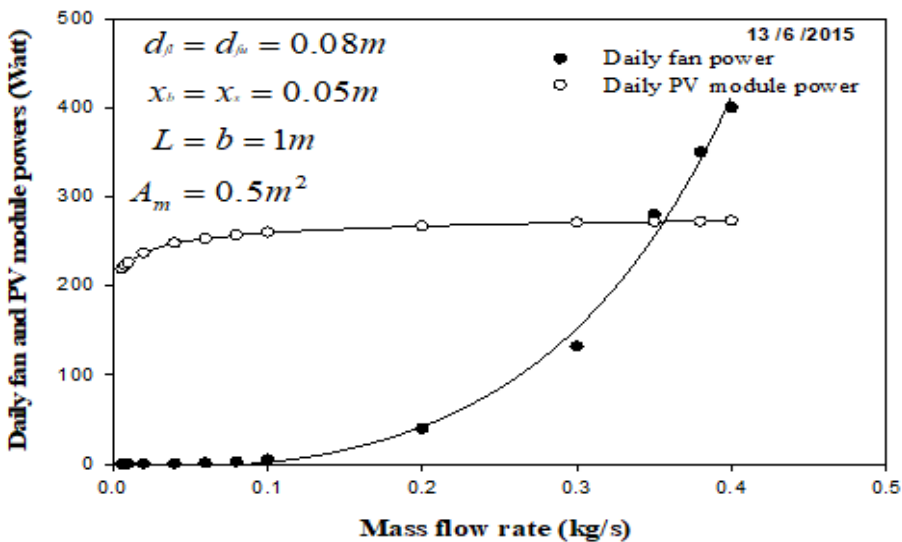


Fig.9 Variations of the daily fan and module powers with \dot{m}

Fig.10. shows variations of the electro-hydraulic efficiency η_{e-h} and the net available electrical power \dot{Q}_{NET} for different values of \dot{m} . Clearly, \dot{Q}_{NET} and η_{e-h} increase until \dot{m} reaches 0.1 kg/s beyond which \dot{Q}_{NET} and η_{e-h} tend to decrease. By increasing \dot{m} , the electro-hydraulic efficiency takes a steep downward path and this is due to the requirement of the fan power increases with increasing \dot{m} , and according to Eqs.(54) and (55), when the power of the fan exceeds net power, the electro-hydraulic efficiency decreases sharply. This result shows a good agreement with Hegazy [5].

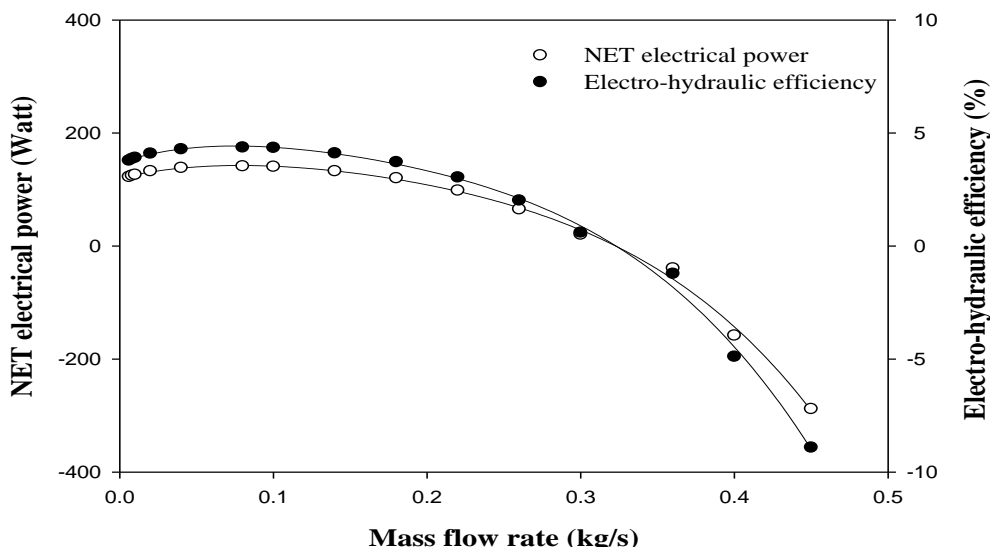


Fig.10 Variation of the electro-hydraulic efficiency and the net electrical power with \dot{m} .

4.5. Effect of the packing factor $F = (A_c/A_p)$.

Figure 11 presents the impact of the packing factor on electrical, thermal and overall efficiencies. Clearly, the increase in the packing factor causes an increase in η_E due to the increased area of the module. With increasing F , η_T decreases due to the decreased collector area. The figure shows that as the packing factor increases from 0.2 to 1, $\eta_{overall}$ decreases from 74 to 67%.

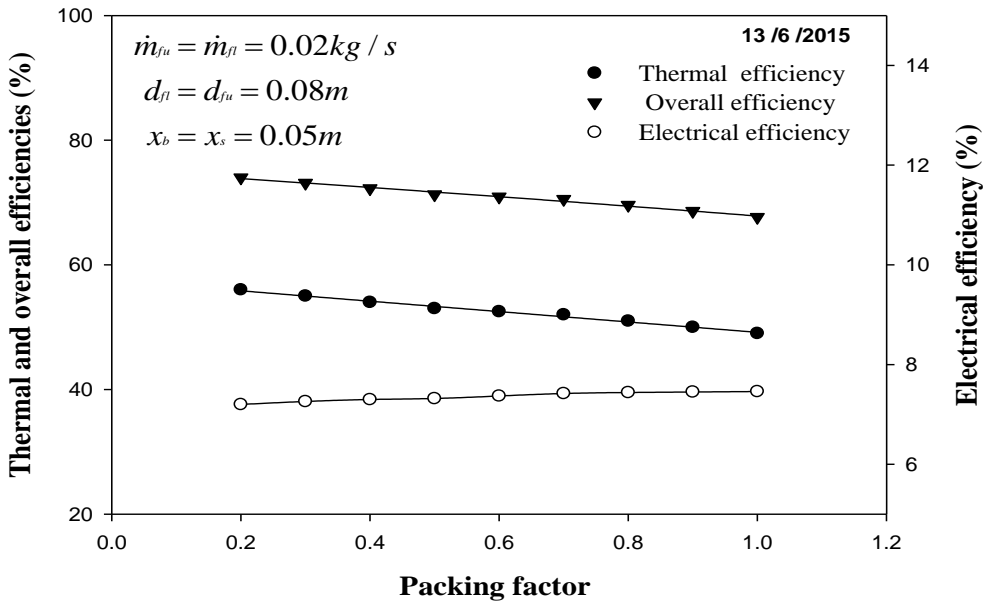


Fig.11 Impact of the packing factor on electrical, thermal and overall efficiencies.

4.6 calculations of the top losses

Fig.12 introduces the change of the top loss coefficient with the time of the day. It is apparent that the top heat losses in the case of the collector without fins are higher than that of the collector with fins. This result because the fins develop the heat transfer rate and consequently reduce the top losses.

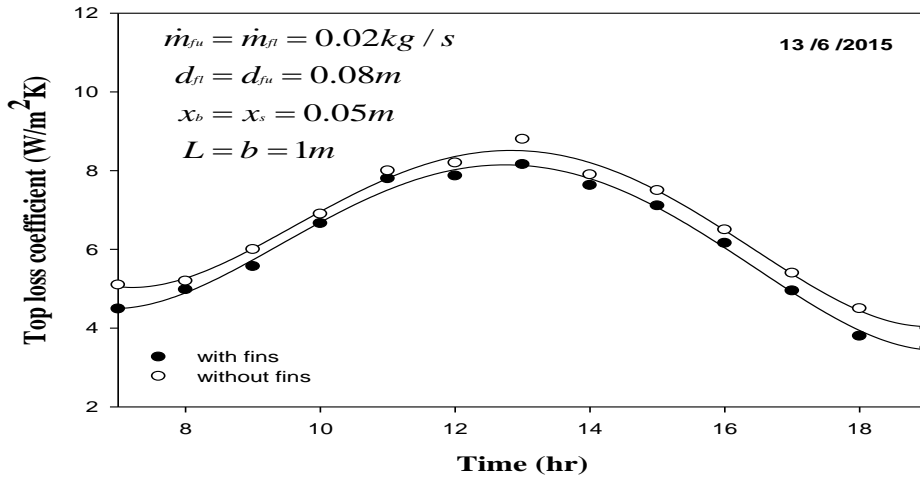


Fig.12 Variation of the top loss coefficient with time

Figure 13 shows the variation of η_T with A_c with and without fins when $\dot{m}_{fu} = \dot{m}_{fl} = 0.02 \text{ kg/s}$, $L = b = 1 \text{ m}$, $A_m = 0.5 \text{ m}^2$, $d_{fu} = d_{fl} = 0.08 \text{ m}$ and $x_b = x_s = 0.05 \text{ m}$. From the results of Fig.13, it can be seen that η_T decreases with increasing A_c and this is due to the opposite proportionality A_c and η_T according to equation (42).

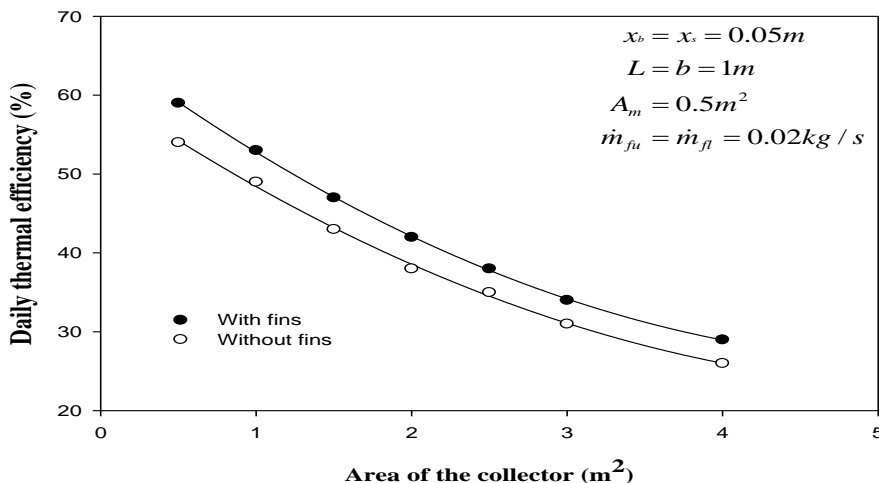


Fig.13. Variations of η_T with A_c

Variation of η_T at different values of the upper channel depth d_{fu} is shown in figure 14, when $\dot{m}_{fu} = \dot{m}_{fl} = 0.02 \text{ kg/s}$, $L = b = 1 \text{ m}$, $A_m = 0.5 \text{ m}^2$, $d_{fl} = 0.016 - d_{fu} \text{ m}$ and $x_b = x_s = 0.05 \text{ m}$. The outcomes of figure 14 indicate that η_T increases by increasing d_{fu} or decreasing d_{fl} .

Figure 15 presents the variation of η_T with the reduced parameter $(T_{f1o} - T_{f1i})/I$. According to figure 15 and Eq. (42), the intercept of the straight line refers to the optical efficiency $(\alpha_p \tau_g)$ which is equal to 0.79 and the slope of the line is the overall losses U_l that obtained as $13.5 \text{ (W/m}^2 \text{ K)}$.

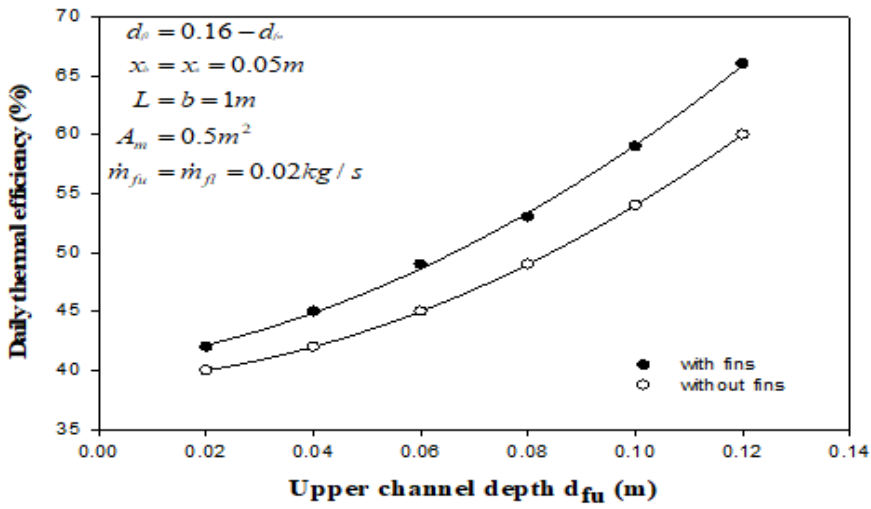


Fig.14. Variations of η_T with d_{fu} .

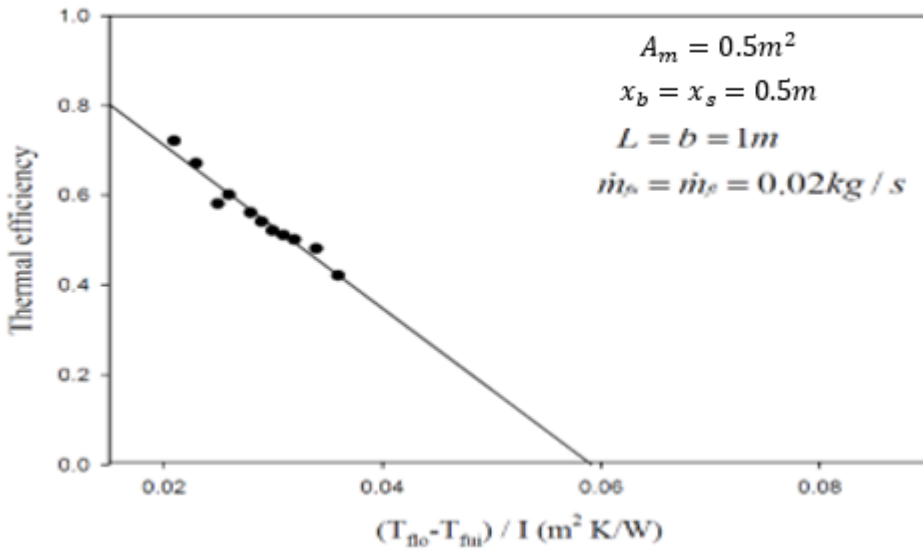


Fig.15. Variations of η_T with the reduced parameter

4.8 Validation of the proposed model

Figures 16 and 17 present a comparison between the present study and a study by Hegazy [5] in order to certify the veracity of the proposed model. Figure 16 introduces a comparison between the daily PV module powers of the present study and Hegazy [5] at different specific \dot{m} when the collector area is 9 m^2 and the PV module area is 8.5 m^2 . We found convergence in the results with a deviation about 10%.

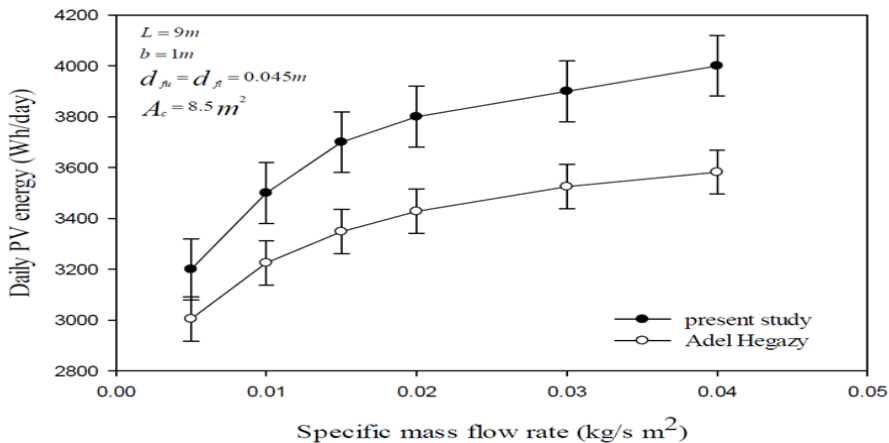


Fig.16. Comparison between the daily PV module energy of the present study and a study made by Hegazy [5].

Figure 17 displays a comparison between the daily fan power at different values of \dot{m} for the current study and another study presented by Hegazy [5]. From the displayed figure, we can say that there is a great agreement in the results of the two studies.

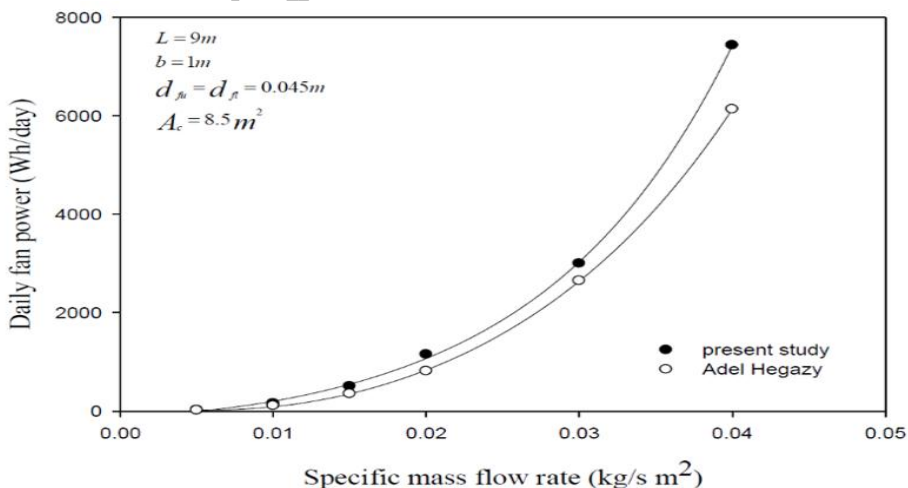


Fig.17. Comparison between the daily fan power of the present study and a study made by Hegazy [5].

5. Conclusion

After investigating the performance of the hybrid PV/T solar air heater and studying the PV module effect and the presence of the fins, we can summarize the following conclusions:

- 1- The PV module can supply electricity to actuate the pump and blow air through the heater until \dot{m} reaches 0.37 kg/s, then the power of the fan goes over the module power. Thus, we cannot operate this heater at \dot{m} higher than 0.37 kg/s.
- 2- There is a reduction in the outlet temperature $T_{f_{lo}}$ about 7.8% in the attendance of the PV module.
- 3- The presence of the fins can boost the electrical and thermal efficiencies by about 10% and 8%, respectively.
- 4- The electro-hydraulic efficiency increases at \dot{m} less than 0.1 kg/s but at higher \dot{m} it takes a steep downward path.

Nomenclature

A	Area of the surface (m^2)
b	Heater width (m)
c	Specific heat (J/kg K)
d	Air channel depth (m)
H	fin height (m)
h	Heat transfer coefficient ($W/m^2 K$)
I	Solar irradiance (W/m^2)
k	Thermal conductivity ($W/m K$)
L	Heater Length (m)
\dot{m}	Air mass flow rate (kg/s)
P	Power (W)
ΔP	Pressure drop (N/m^2)
\dot{Q}_u	output thermal power (W)
\dot{Q}_p	output electrical power (W)
t	Fin thickness (m)
x	Insulation thickness (m)
A_c	PV module area (m^2)
t	fin thickness (m)

Subscript

a	Ambient
b	Back
c	Convective
f	Fluid
g	Glass

<i>i</i>	Inlet
<i>l</i>	Lower
<i>o</i>	Outlet
<i>p</i>	Absorber plate
<i>r</i>	Radiative
<i>s</i>	Sky, side
<i>w</i>	wind
<i>u</i>	Upper
DPFPSAH Double pass finned plate solar air heater	

Greek

α	Absorptivity
τ	Transmissivity

Appendix A.

$$r_1 = h_w + h_{r_{gs}} + h_{cg} + h_{r_{pg}}$$

$$r_2 = h_{p1} + h_{p2}\phi + h_{r_{pg}} + h_{r_{pb}}$$

$$r_3 = U_b + h_b + h_{r_{pb}}$$

$$r_4 = 1 - \frac{h_{r_{pb}}^2}{r_2 r_3}$$

$$r_5 = r_2 r_3 r_4$$

$$r_6 = 1 - \frac{r_3 h_{r_{pg}}^2}{r_1 r_5}$$

$$r_7 = r_1 r_5 r_6$$

$$r_8 = \frac{r_3 S_p}{r_5}$$

$$r_9 = \frac{r_3 h_{p1}}{r_5}$$

$$r_9 = \frac{r_3 h_{p1}}{r_5}$$

$$r_{10} = \frac{r_3 h_{p2}\phi}{r_5}$$

$$r_{11} = \frac{h_{r_{pb}} h_b}{r_5}$$

$$r_{12} = \frac{U_b h_{rpb}}{r_5}$$

$$r_{13} = \frac{r_3 h_{rpg}}{r_5}$$

$$r_{14} = \frac{h_b}{r_3}$$

$$r_{15} = \frac{U_b}{r_3}$$

$$r_{16} = \frac{h_{rpb}}{r_3}$$

$$n_1 = \frac{(r_5 I \alpha_g + h_{rpg} r_3 S_p)}{r_7}$$

$$n_2 = \frac{r_5 h_{cg} + h_{rpg} r_3 h_{p1}}{r_7}$$

$$n_3 = \frac{r_3 h_{rpg} h_{p2} \phi + h_{rpg} h_{rpb} h_b}{r_7}$$

$$n_4 = \frac{r_5 h_w + h_{rpg} U_b h_{rpb}}{r_7}$$

$$n_5 = \frac{r_5 h_{rgs}}{r_7}$$

$$n_6 = r_8 + (r_{13} n_1)$$

$$n_7 = r_9 + (r_{13} n_2)$$

$$n_8 = r_{10} + r_{11} + (r_{13} n_3)$$

$$n_9 = r_{12} + (r_{13} n_4)$$

$$n_{10} = r_{13} n_5$$

$$n_{11} = r_{16} n_6$$

$$n_{12} = r_{16} n_7$$

$$n_{13} = r_{14} + r_{16} n_8$$

$$n_{14} = r_{15} + r_{16} n_9$$

$$n_{15} = r_{16}n_{10}$$

Appendix B

$$S_1 = \frac{b}{(\dot{m}_{fu}C_{fu})}$$

$$A_1 = S_1[h_{p1}(1 - n_7) + h_{cg}(1 - n_2) + U_s]$$

$$E_1 = S_1[h_{p1}n_8 + h_{cg}n_3]$$

$$f_1(t) = S_1[(h_{p1}n_6 + h_{cg}n_4) + (h_{p1}n_9 + h_{cg}n_4 + U_s)T_a + (h_{p1}n_{10} + h_{cg}n_5)T_s]$$

$$S_2 = \frac{b}{(\dot{m}_{fl}C_{fl})}$$

$$A_2 = S_2[h_b(1 - n_{13}) + h_{p2}\phi(1 - n_8) + U_s]$$

$$E_2 = S_2(h_{p2}\phi n_7 + h_b n_{12})$$

$$f_2(t) = S_2[(\phi h_{p2}n_6 + h_b n_{14}) + (h_{p2}\phi n_9 + h_b n_{14} + U_s)T_a + (\phi h_{p2}n_{10} + h_b n_{15})T_s]$$

References

- [1] F. Hussain, M. Y. H. Othman, B. Yatim, H. Ruslan, K. Sopian, and Z. Anuar, "An improved design of photovoltaic/thermal solar collector," *Sol. Energy*, vol. 122, pp. 885–891, 2015.
- [2] J. Kim, S. Park, and J. Kim, "Experimental performance of a photovoltaic-thermal air collector," *Energy Procedia*, vol. 48, pp. 888–894, 2014.
- [3] L. J. Huang and R. K. Shah, "Assessment of calculation methods for efficiency of straight fins of rectangular profile," *Int. J. Heat Fluid Flow*, vol. 13, no. 3, pp. 282–293, 1992.
- [4] O. K. Ahmed, Z. A. Mohammed, and O. K. Ahmed, "Dust effect on the performance of the hybrid PV / Thermal collector," *Therm. Sci. Eng. Prog.*, no. July 2017.
- [5] A. A. Hegazy, "Comparative study of the performances of four photovoltaic /thermal solar air collectors," *Energy Convers. Manag.*,

vol. 41, 2000.

- [6] J. S. Coventry, "Performance of a concentrating photovoltaic/thermal solar collector," *Sol. Energy*, vol. 78, pp. 211–222, 2005.
- [7] A. Shahsavari and M. Ameri, "Experimental investigation and modeling of a direct-coupled PV / T air collector," *Sol. Energy*, vol. 84, no. 11, pp. 1938–1958, 2010.
- [8] O. K. Ahmed and Z. A. Mohammed, "Influence of porous media on the performance of hybrid PV/Thermal collector," *Renew. Energy*, vol. 112, pp. 378–387, 2017.
- [9] S. Dubey, G. S. Sandhu, and G. N. Tiwari, "Analytical expression for electrical efficiency of PV / T hybrid air collector," *Appl. Energy*, vol. 86, no. 5, pp. 697–705, 2009.
- [10] M. Yusof, H. Othman, B. Yatim, K. Sopian, M. Nazari, and A. Bakar, "Performance analysis of a double-pass photovoltaic/thermal (PV / T) solar collector with CPC and fins," *Renew. Energy*, vol. 30, no. 2005, pp. 2005–2017, 2017.
- [11] A. Tiwari and M. S. Sodha, "Parametric study of various configurations of hybrid PV / thermal air collector : Experimental validation of theoretical model," *Sol. Energy Materials & Sol.Cells*, vol. 91, pp. 17–28, 2007.
- [12] S. Dubey and G. N. Tiwari, "Thermal modeling of a combined system of photovoltaic thermal (PV / T) solar water heater," *Sol. Energy*, vol. 82, pp. 602–612, 2008.
- [13] H. M. Yeh, C. D. Ho, and J. Z. Hou, "Collector efficiency of double-flow solar air heaters with fins attached," *Energy*, vol. 27, no. 8, pp. 715–727, 2002.
- [14] J. A. Duffie and W. A. Beckman, *Solar engineering of thermal processes*, 4th Edition, John Wiley & Sons, New York (2013).
- [15] C. D. Ho, H. M. Yeh, and R. C. Wang, "Heat-transfer enhancement in double-pass flat-plate solar air heaters with recycle," *Energy*, vol. 30, pp. 2796–2817, 2005.
- [16] F. K. Forson, M. a. a. Nazha, and H. Rajakaruna, "Experimental and simulation studies on a single pass, double duct solar air-heater.," *Energy Convers. Manag.*, vol. 44, pp. 1209–1227, 2003.
- [17] H. Heaton, W. C. Reynolds, and W. M. Kays, "Heat transfer

- simultaneous temperature,” *Ink J. Heat Mass Transf.*, vol. 7, pp. 763–781, 1964.
- [18] K. S. Ong and E. B. Norton, “Thermal performance of solar air heaters : mathematical model and solution procedure” *Sol. Energy*, vol. 55, no. 2, pp. 93–109, 1995.
- [19] H. Yeh, C. Ho, and C. Lin, “Effect of collector aspect ratio on the collector efficiency of upward type baffled solar air heaters,” *Energy Convers. Manag.*, vol. 41, pp. 971–981, 2000.
- [20] W. E. Boyce, "Elementary Differential Equations and Boundary Value Problems," *Wily*, vol. 53, no. 9. 2013.
- [21] J. D. Anand, D. K. Dutt, A. Kumar, and G. N. Tiwari, “Improved Design of a Double Effect Solar Still,” *Energy Convers. Mgmt*, vol. 34, no. 6, pp. 507–517, 1993.
- [22] R. Chandra, V. K. Goel, and B. C. Raychaudhuri, “Performance comparison of two-pass modified reverse flat-plate collector with conventional flat-plate collectors,” *Energy Convers. Manag.*, vol. 23, no. 3, pp. 177–184, 1983.
- [23] A. A. Hegazy, “Thermohydraulic performance of air heating solar collectors with variable width, flat absorber plates,” *Energy Convers. Manag.*, vol. 41, no. 13, pp. 1361–1378, 2000.
- [24] D. Su, Y. Jia, X. Huang, G. Alva, Y. Tang, and G. Fang, “Dynamic performance analysis of photovoltaic – thermal solar collector with dual channels for different fluids,” *Energy Convers. Manag.*, vol. 120, pp. 13–24, 2016.
- [25] A. S. Joshi, A. Tiwari, G. N. Tiwari, I. Dincer, and B. V Reddy, “Performance evaluation of a hybrid photovoltaic thermal (PV / T) (glass-to-glass) system,” *Int. J. Therm. Sci.*, vol. 48, no. 1, pp. 154–164, 2009.
- [26] Griggs EI, Sharifabad FK. Flow characteristics in rectangular ducts. *ASHRAE Trans*; 98(1):116±27,1992.
- [27] R. L. Daughery, J.B. Franzini and E. J. Finnemore, fluid mechanics with engineering applications. McGraw Hill, p. 293-(1989).
- [28] R. Kumar and P. Chand, “Performance enhancement of solar air heater using herringbone corrugated fins,” *Energy*, vol. 127, pp. 271–279, 2017.

- [29] C. D. Ho, H. M. Yeh, T. W. Cheng, T. C. Chen, and R. C. Wang, "The influences of recycle on performance of baffled double-pass flat-plate solar air heaters with internal fins attached," *Appl. Energy*, vol. 86, no. 9, pp. 1470–1478, 2009.
- [30] D. Alta, E. Bilgili, C. Ertekin, and O. Yaldiz, "Experimental investigation of three different solar air heaters: Energy and exergy analyses," *Appl. Energy*, vol. 87, no. 10, pp. 2953–2973, 2010.
- [31] Kumar, R., Rosen, M. Performance evaluation of a double pass PV/T solar air heater with and without fins. *Appl. Therm. Eng.* 31, 1402–1410, 2011.

Egypt. J. Solids